

# AA6082 to DX56-Steel Laser Brazing: Process Parameter–Intermetallic Formation Correlation

D. Narsimhachary, S. Pal, S.M. Shariff, G. Padmanabham, and A. Basu

(Submitted January 9, 2017; in revised form June 1, 2017; published online September 5, 2017)

In the present study, laser-brazed AA6082 to DX56-galvanized steel joints were investigated to understand the influence of process parameters on joint strength in terms of intermetallic layer formation. 1.5-mm-thick sheet of aluminum alloy (AA6082-T6) and galvanized steel (DX56) sheet of 0.7 mm thickness were laser-brazed with 1.5-mm-diameter Al-12% Si solid filler wire. During laser brazing, laser power (4.6 kW) and wire feed rate (3.4 m/min) were kept constant with a varying laser scan speed of 3.5, 3, 2.5, 2, 1.5, and 1 m/min. Microstructure of brazed joint reveals epitaxial growth at the aluminum side and intermetallic layer formation at steel interface. Intermetallic layer formation was confirmed by EDS analysis and XRD study. Hardness profile showed hardness drop in filler region, and failure during tensile testing was initiated through the filler region near the steel interface. As per both experimental study and numerical analysis, it was observed that intermetallic layer thickness decreases with increasing brazing speed. Zn vaporization from galvanized steel interface also affected the joint strength. It was found that high laser scan speed or faster cooling rate can be chosen for suppressing intermetallic layer formation or at least decreasing the layer thickness which results in improved mechanical properties.

**Keywords** AA6082, brazing, diffusion, dissimilar-joint, DX56-steel, interfacial conductivity, intermetallics, laser

## 1. Introduction

Partial replacement of steel in the automotive industry by aluminum alloys became a common practice for achieving lower specific weight, which in turn increases fuel efficiency and accordingly reduces the greenhouse effect. This necessitates attainment of proper mechanical properties of aluminum to steel joint, which can also widen the application domain of components made by such aluminum-steel hybrid structure (Ref 1, 2). However, joining of dissimilar materials like aluminum to steels is challenging due to variation in their thermo-physical (density, specific heat, thermal and electrical conductivity) and metallurgical characteristics (Ref 3). Low solubility between Fe and Al causes intermetallic formation during solidification in case of fusion welding (Ref 4). Moreover,  $Fe_xAl_y$  intermetallic compounds (IMC) are brittle in nature and exhibit wide variation in mechanical properties even by slight change in their stoichiometry. For example, Fe-rich  $Fe_3Al$  shows hardness of 250–350 HV, whereas Al-rich  $FeAl_3$  displays 820–980 HV hardness (Ref 5). Therefore, complete elimination of intermetallics or inhibition of intermetallic formation is recommended; however, reduction in intermetallic layer thickness may be the alternative and realistic option. In addition to this, other issues like distortion, cracking

and porosity in the fusion zone are of concerns during joining of aluminum to steel.

To reduce problems associated with IMC, some of the researchers adopted solid state joining techniques like resistance welding (Ref 6), diffusion bonding (Ref 7) and friction stir welding (Ref 8). Joints obtained by these processes have better mechanical properties, as these joints contain significantly low intermetallic layer thickness. However, the application domain of these techniques is restricted to special types of work pieces, joint designs and backing plates.

Conventional arc weld-brazing process such as metal arc weld brazing (MAW) and Tungsten inert gas weld brazing (TIG) leads to formation of brittle intermetallics having thickness ranging from 5 to 40  $\mu\text{m}$  due to higher heat input associated with such techniques (Ref 9). On the other hand, cold metal transfer process displays improved joint efficiency, but this can be used only for thin plates (Ref 10). Moreover, this process also has limitation of lower welding speed. A joining process having lower as well as concentrated localized heat input can increase joint efficiency by decreasing intermetallic layer thickness, distortion and residual stress. In this connection, laser brazing can be chosen as a tool for joining of Al to Steel due to its unique heat input features.

In laser brazing, temperature and viscosity play a major role in wetting of the filler metal, and to avoid the problems related to incompatibility, proper parameters are to be chosen (Ref 11). To minimize the thickness of intermetallic layer as well as to improve the efficiency of joints, temperature versus time distribution at the interface area should be optimized by controlling the process parameters. This necessitates the investigation of IMC layer formation mechanism and prediction of its thickness with respect to the process parameters of laser brazing.

The effect of laser brazing process parameters on the joint strength by virtue of intermetallic formation mechanism has been discussed in the present study. Moreover, a predictive model, based on close coordination between experimental investigation and theoretical calculations, was made to identify the relation

D. Narsimhachary, S. Pal, and A. Basu, Department of Metallurgical and Materials Engineering, National Institute of Technology, Rourkela, Odisha 769008, India; and S.M. Shariff and G. Padmanabham, International Advanced Research Centre for Powder Metallurgy & New Materials (ARCI), Hyderabad, Telangana 500005, India. Contact e-mail: anindya.basu@gmail.com and basua@nitrrkl.ac.in.

between intermetallic layer thickness and process parameters during laser brazing of AA6082 to DX56 (galvanized) steel.

## 2. Experimental

### 2.1 Materials and Method

Aluminum alloy (AA6082-T6) sheet of 1.5-mm-thick, galvanized steel (DX56) sheet of 0.7-mm-thick and 1.5-mm-diameter solid AA4047 filler wire were used in the present study. The nominal chemical composition of AA6082-T6 was 0.40% Mn; 0.50% Fe; 0.7-1.3% Si; 0.10% Cu; 0.25% Cr; 0.20% Zn; 0.006-1.20% Mg; balance Al (in wt. %), DX56 was 0.02% C; 0.25% Mn; 0.02% P; 0.02% S; 0.30% Ti; balance Fe and filler wire AA4047 was 0.55% Mn; 0.6% Fe; 10.5-13.5% Si; 0.15% Mg; balance Al. Aluminum alloy and steel pieces were machined in 150 mm × 100 mm dimension from the above-mentioned sheets to perform the joining experiments with T joint (fillet) configuration. The edges of the samples were ground and cleaned with wire brush and followed by acetone wash to remove oxide layer and grease before joining.

A diode laser (LDF 6000) with 6 kW maximum power was used in the experiment. Inert gas (Argon) was fed through a 10-mm nozzle at a flow rate of 0.5 bar in the trailing mode configuration. During the trials, laser speed was varied (3.5, 3, 2.5, 2, 1.5, and 1 m/min), whereas other process parameters like laser power (4.6 kW) and wire feed rate were kept constant (3.4 m/min).

### 2.2 Characterizations

The brazed joints were cross-sectioned using abrasive cutting machine, mounted and polished for macroscopic and microscopic characterization. The mounted specimens were polished by successive grades of emery papers followed by cloth polishing with alumina powder. Finally, the specimens were cleaned and were subjected to chemical etching using Keller's reagent (2.5 mL HNO<sub>3</sub>, 1.5 mL HCl, 1 mL HF in 95 mL of H<sub>2</sub>O). Macro and microstructural images of brazed zone and base material (BM) were analyzed by stereo zoom and optical microscope (Carl Zeiss). JEOL JSM-6084LV scanning electron microscope (SEM) fitted with EDS (Oxford, INCAx-act, Model No: 51-ADD0013) attachment was also used to study the microstructural and elemental analysis. The brazed joints were subjected to XRD analysis using Cu K<sub>α</sub> target in Rigaku JAPAN/ULTIMA-IV x-ray diffractometer. Microhardness measurements were conducted on brazed sections using Vickers microhardness tester (IMS UHL 5.0, WALTER UHL, Germany) fitted with Vickers diamond indenter. A load of 50 g and a residence time of 15 s were maintained for all measurements. An average of minimum five hardness readings was reported as a single hardness value. The joints were characterized for tensile testing using INSTRON, SATEC 600 kN instrument with a cross head velocity of 1 mm/min. The 'load to fracture' value reported here is an average of results obtained from tensile tests of three identical specimens.

## 3. Results and Discussion

### 3.1 Microstructure

Macrostructural study was carried out for detecting macro-scale defects, and the same is presented in Fig. 1. The

macrostructures depict that the joints were free from both macroporosity and cracks. From the figure, it was also found that with change in scan speed there was variation in the root gap filling by molten filler. At higher scan speed, coverage by molten filler was poor due to faster melting and solidification rate. From the figure, it can be estimated that, with 3.0 m/min scan speed, the gap was ~1.5 mm; but in case of 1.0 m/min scan speed, it was only ~0.6 mm.

Representative optical microstructures of laser-brazed joint prepared using 4.6 kW laser power, 3.5 m/min brazing speed and 3.4 m/min wire feed rate are presented in Fig. 2. It displays the fusion zone and interface between filler material and aluminum (Fig. 2a) as well as the interface of filler material and steel (Fig. 2c). The microstructure of fusion zone exhibits fine dendritic structure as this zone has undergone through melting followed by high rate of cooling. There was no evidence of melting of base material at the fusion zone–steel interface (Fig. 2c), which confirms the conventional brazing mechanism. On the other hand, epitaxial growth was observed at interface between fusion zone and aluminum base material as evident in Fig. 2(a). Melting of base material (Al alloy) near the interface is necessary for epitaxial growth (Ref 12), which evidently justifies partial melting of aluminum alloy near the interface. This phenomenon is unlikely for conventional laser brazing. So, it can be inferred that welding was taken place at aluminum side, whereas, for steel side, brazing was the sole joining mechanism. Presence of minor porosity on the aluminum interface can be attributed to hydrogen entrapment in the melt pool as enough time for escape was not available due to high laser brazing speed (Ref 13).

SEM micrographs of laser-brazed joint, prepared with 4.6 kW power, 3.4 m/min wire feed rate, and 3.5 m/min scan speed are presented in Fig. 3. Existence of intermetallic layer was observed on the steel interface. Moreover, observation along this interface reveals that intermetallic layer growth can be categorized into different modes. At first, intermetallic layer grew in planar mode just adjacent to the steel and then it was changed to cellular/dendritic mode; and lastly, it was segregated as small cuboid shapes in the molten filler due to variation in heat dissipation. EDS analysis was carried out at different places (marked as 1-4 in Fig. 3) on the steel interface of the brazed joint to get an idea about the intermetallics composition and the same is summarized in Table 1. On the basis of estimated stoichiometry, obtained EDS results of point 1 and 4 represent Fe<sub>2</sub>Al<sub>5</sub>. Formation of such intermetallics at reaction layer was also reported earlier (Ref 14, 15). Intermetallic layer formation at the Galvanized steel (solid)/Al-12Si (liquid) interface during laser brazing can be initiated by dissolution of iron atom at the molten filler pool and subsequent diffusion of the same away from the interface. During solidification, first Fe<sub>2</sub>Al<sub>5</sub> phase may have formed at the interface due to its lower Gibbs free energy and higher melting point (1169 °C) than Fe<sub>3</sub>Al (Ref 16). The solubility of Fe in Al decreases gradually as the temperature decreases and so, lastly, it was precipitated by formation of aluminum-rich intermetallic (Fe<sub>3</sub>Al). Minor amount of zinc was also detected mainly in brazed zone as well as in intermetallics. This zinc atom can also substitute aluminum atom in the final intermetallic compound as Fe<sub>2</sub>Al<sub>5</sub>Zn<sub>0.4</sub> (Ref 16).

### 3.2 XRD

XRD analysis was performed on the laser-brazed joints to find the existence of Intermetallic phase at the steel interface, and the



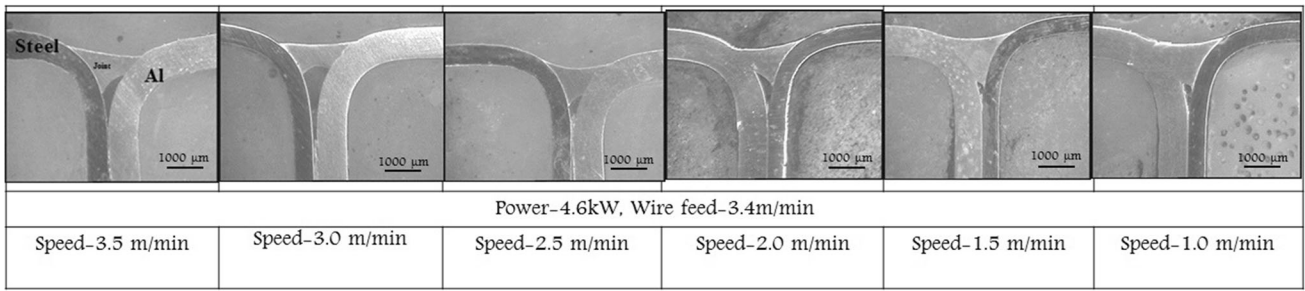


**Fig. 1** Macrostructure of fillet joints with varying speed

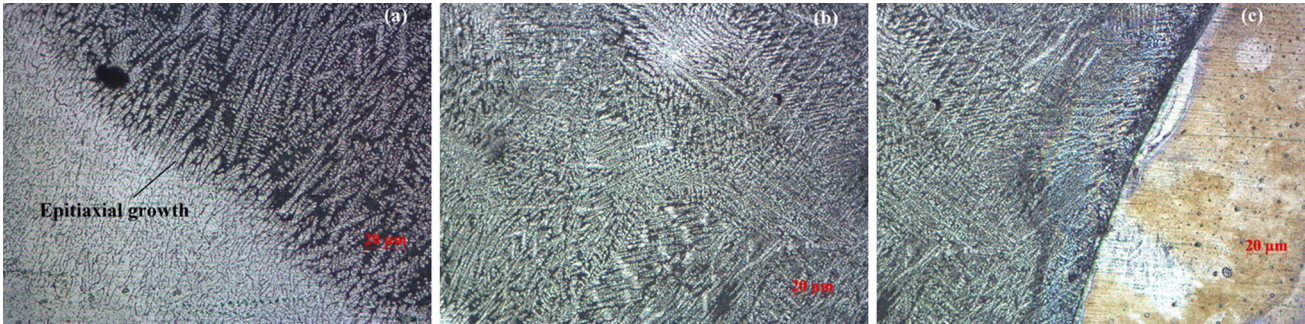


**Fig. 2** Microstructure of joints (a) aluminum side interface, (b) fusion zone, and (c) steel side interface

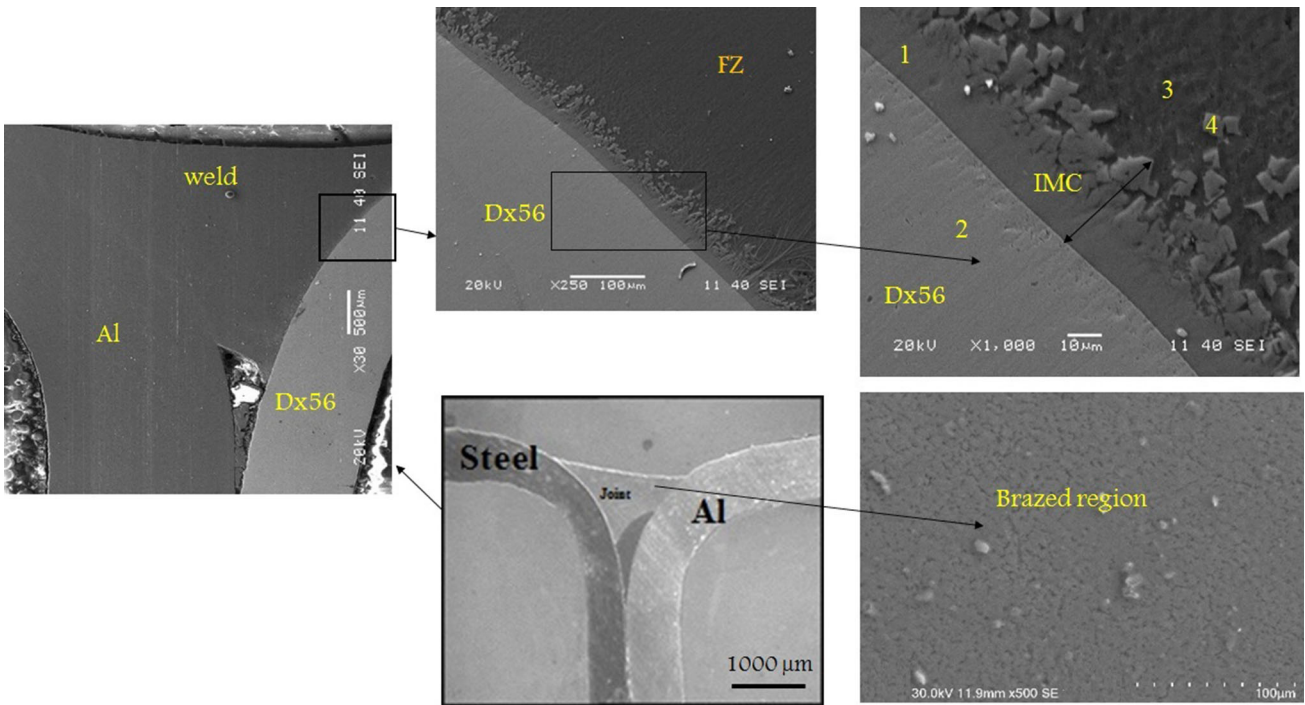


**Fig. 3** SEM microstructure of joints (4.6 kW Power, 3.5 m/min speed)

same is reported in Fig. 4. From the XRD results, it is evident that along with Al- and Fe-rich phases, intermetallic peaks are also present. XRD pattern of the joint reveals marginally strong Al-rich intermetallic peaks of  $\text{Fe}_2\text{Al}_5$  ( $\eta$ -phase) and  $\text{FeAl}_3$  ( $\theta$ -phase). The profile also shows weak peak of Fe-rich  $\text{Fe}_3\text{Al}$  that may be due to its small fraction at the interface.

### 3.3 Hardness

Microhardness measurements were carried out on the transverse sections of the joints, and the values were plotted across the width maintaining relative length scale. Figure 5 shows such plot of two extreme laser scan speeds (1 and 3.5 m/

**Table 1 EDS analysis**

Point no.	at. %				Possible intermetallic
	Al	Si	Fe	Zn	
1	65.58	7.90	25.94	0.58	Fe <sub>2</sub> Al <sub>5</sub>
2	...	...	98.37	1.63	...
3	86.23	11.84	1.13	0.8	...
4	67.6	6.02	25.88	0.5	Fe <sub>2</sub> Al <sub>5</sub>

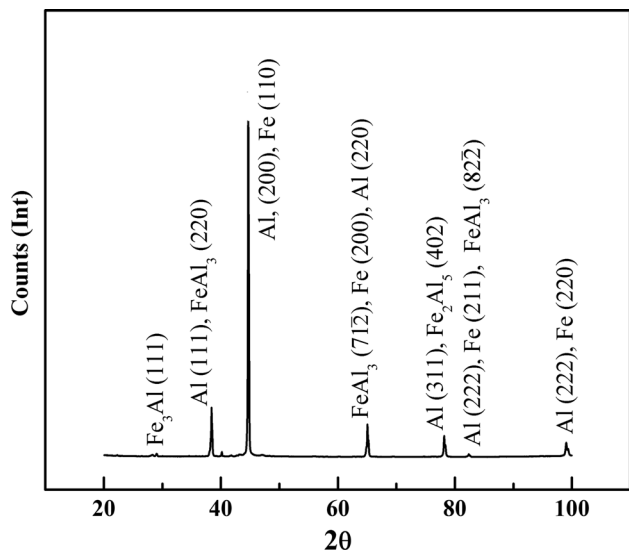


**Fig. 4** XRD analysis of laser-brazed joint (3.5 m/min speed)

min). The average hardness of the Al alloy and galvanized steel were 110 and 165 Hv, respectively. Brazed zone has lower hardness value in both the samples compared to the base materials. Marginal higher hardness was observed in laser-brazed joint prepared with 3.5 m/min speed, mainly due to its finer structure for higher cooling rate. Presence of heat-affected zone (HAZ) could not be ascertained from the microstructure, whereas from the hardness plot it was found that there exists a HAZ mainly at the Al side. Identifying IMC layer under optical microscope during microhardness measurement was not easy and the size of microhardness indenter was too large to specifically measure the hardness of the thin IMC layer without surrounding. So, specific hardness values of the intermetallics at the steel interface could not be reported.

### 3.4 Tensile Testing

Tensile tests were conducted on brazed joint specimens to investigate the strength of the same and the results are shown in Fig. 6(a). The figure reveals that, with increasing laser scan speed, the load bearing capacity of the joint increases. This may be attributed to finer structure due to faster cooling or intermetallic formation related mechanism. Figure 6(b) shows a representative macro image of fractured specimen to demonstrate the position of the fracture location. It reveals that the initiation and propagation of crack was through the interface of brazed zone and steel interface.

Figure 7 shows the SEM micrographs of fractured surfaces of aluminum side as well as galvanized steel side. These

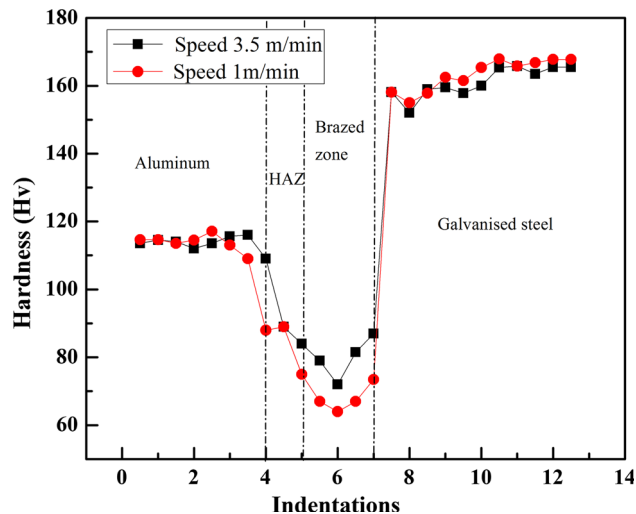


**Fig. 5** Microhardness profiles of laser-brazed joints with varying speed (1 and 3.5 m/min)

fracture surfaces were obtained from the tensile test as mentioned above, and the figure demonstrates one such sample prepared with laser scan speed of 3.5 m/min. The crack was initiated from the weld root and propagated through the brazed/fusion zone because of its cast structure. The fractured surface of the top of the aluminum side (near the root) revealed mainly ductile mode of fracture with dimple morphology (Fig. 7a). The steel side also demonstrates similar morphology (Fig. 7b). This may be due to the reason that the failure was not exactly on the intermetallic layer but perhaps on the junction of the cast filler structure to intermetallic layer as seen in Fig. 6(b) macrograph.

The fractured surface of the bottom of the aluminum side also revealed ductile mode of fracture with presence of large dimples (Fig. 7c). This is due to the presence of micropores or change in cast structure from top to bottom portion of the joint. Bottom portion of the steel side also exhibited similar structure (Fig. 7d). But number of large dimples/voids is marginally higher at the steel side. Evaporation of Zn from the galvanized coating caused by laser brazing may attribute to this effect.

### 3.5 Cooling Rate Calculation

Microstructure of a brazed region is highly dependent on the maximum temperature and cooling rate experienced by that region, because thermodynamic feasibility is governed by temperature, and transformation kinetics is influenced by cooling rate. For the present study, cooling rate was calculated using Eq 1 (Ref 17).



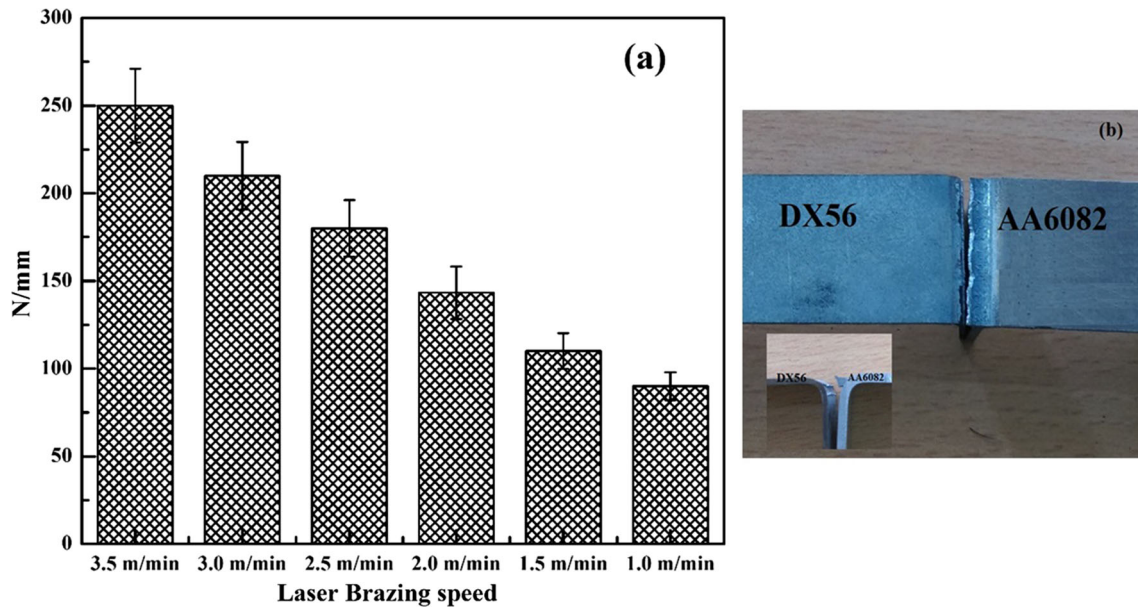


Fig. 6 (a) Load value to fracture of fillet joints with varying laser speed and (b) fracture location of joints

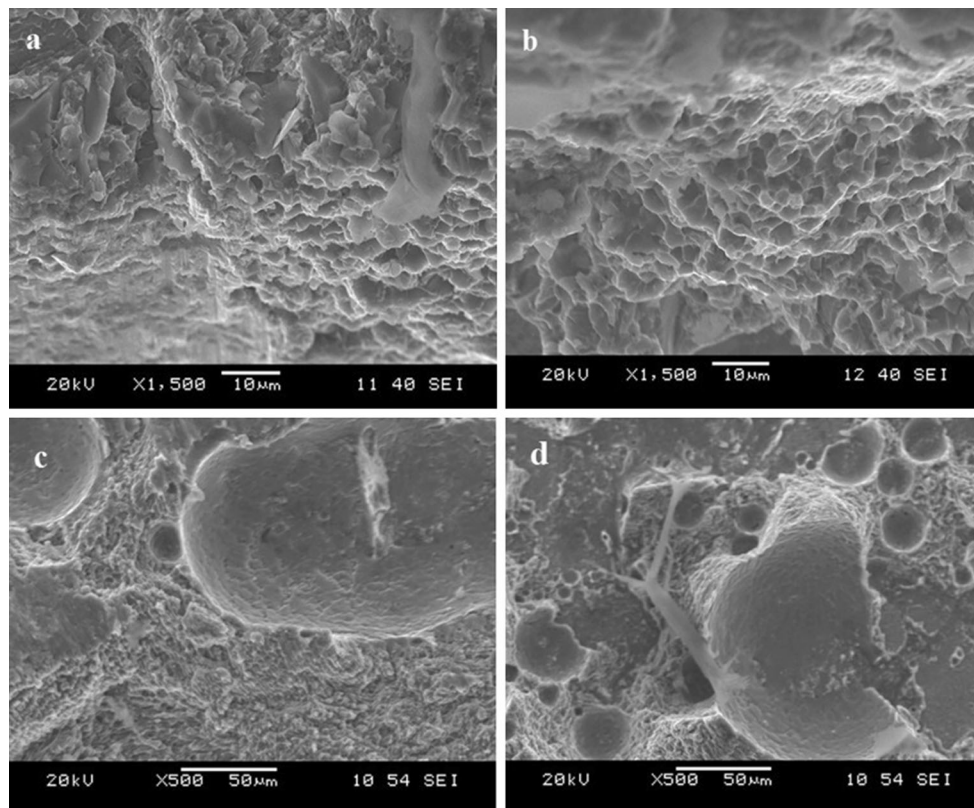


Fig. 7 SEM photographs of fractured surfaces of brazed joints prepared with 3.5 m/min scan speed: (a) top aluminum side, (b) top galvanized steel side, (c) bottom aluminum side and (d) bottom galvanized steel side

$$R = \frac{2\pi k_c (T_c - T_0)^2}{H_{\text{net}}} \quad (\text{Eq 1})$$

where  $R$  = cooling rate at the center line of the weld (K/s),  $k_c$  = thermal conductivity of base material.  $T_0$  = initial plate temperature (K) and  $T_c$  = temperature, where cooling rate was calculated.  $H_{\text{net}}$  can be obtained by Eq 2.

$$H_{\text{net}} = \frac{\text{power } (p)}{\text{speed } (v)} \quad (\text{Eq 2})$$

As thermal conductivity value of the brazed joint across the interface was varied due to dilation, interfacial conductivity was calculated using following relation:

$$\frac{1}{k_c} = \frac{1-f_c}{K_c} + \frac{f_c}{K_E} \quad (\text{Eq 3})$$

where  $K_E$  is thermal conductivity of filler wire (142 W/m K) (Ref 18),  $K_c$  is thermal conductivity of galvanized steel (50 W/m K),  $f_c$  is considered as 0.1 (Ref 19).  $P$  is laser power (4.6 kW),  $v$  is welding speed (3.5 m/min). A region adjacent to steel interface toward center line of the joint was considered for calculation of interfacial conductivity by assigning  $f_c = 0.1$ . The reason for selecting such cross section is to study the effect of cooling/interaction between molten filler and galvanized steel.

From the above-mentioned relation, cooling rate at the steel interface was calculated and plotted versus temperature in Fig. 8(a). It was observed from the figure that cooling rate increases with temperature. The cooling rate versus temperature plot (represented by dotted line) was converted to step function curve taking 200 K for each temperature step, so that for a particular time period, to simplify the relation, temperature can be assumed constant. The residence time for a particular temperature step was calculated, and the same was also plotted with temperature as shown in Fig. 8(a). This approach was meant for obtaining necessary time period for a particular temperature to calculate diffusivity as a function of temperature/time period. Sensitivity analysis was done with different step size, and it was observed that with higher step size the total time duration increases. Therefore, it can be inferred that this kind of calculations are sensitive to step size and accordingly experimental validation for choosing step size is necessary. In this work, step size value was optimized through measuring the surface temperature during periodic time span after passing of laser beam. And it was found that 200 K time step was giving close agreement between observed and calculated time span to reach a particular temperature.

### 3.6 Layer Thickness Measurement

Intermetallic compound formation at the steel-filler interface requires relative movement of aluminum/iron atoms for fulfilling stoichiometric requirement of the specific intermetallic. A

rational effort to estimate the thickness of intermetallic layer by atomic diffusion was reported in the literature (Ref 20). But it does not verify the dependence of intermetallic layer thickness on diffusion distance. Here, first time an attempt was made to correlate the formed intermetallic layer thickness with calculated diffusion distance.

Resultant diffusion distance is calculated by summing up individual diffusion distance ( $x$ ) corresponding to a specific diffusion coefficient ( $D$ ) prevailed for a specific time period ( $t$ ) using the equation  $x = \sqrt{Dt}$ . Furthermore, diffusion coefficient ( $D$ ) at a particular temperature ( $T$ ) can be calculated using  $D = D_0 \exp(\frac{-Q}{RT})$ , where  $D_0$  = pre-exponential constant,  $R$  (8.314 kJ/mol K) is universal gas constant and  $Q$  = activation energy of diffusion.  $D_0$  and  $Q$  values were considered as  $1.91 \times 10^{-8} \text{ m}^2/\text{s}$  and 84.98 kJ/mol (diffusion of iron in aluminum), respectively (Ref 15).

From the time temperature combinations, obtained from Fig. 8(a), time ( $t$ ) and diffusion coefficient ( $D$ ) combinations were calculated. Further, with each of the time and diffusion coefficient combinations, individual diffusion distance was calculated and summing all such individual data, resultant diffusion distance was obtained. Diffusion, being a time-dependent slow process, was calculated during the cooling cycle of the brazing process.

Diffusion distance obtained for each brazing condition is displayed in Fig. 8(b). Thickness of the IMC layer formed across the steel interface was measured from the corresponding micrograph and was also displayed in the same figure. It can be observed that both intermetallic reaction layer thickness and diffusion distance decrease with increasing brazing speed which is at par with the observations reported in literature (Ref 21, 22). High-scan speed results in lower residence time of reaction between metals necessary for intermetallic formation. Therefore, intermetallic layer thickness was observed to be less for higher scan speed. Moreover, wider intermetallic layer at the interface deteriorates mechanical properties (Ref 22-24) of the joint due to its brittle nature. This claim can be justified by the results presented in Fig. 6(a), which evidently shows lower load to fracture for lower scan speed sample. Location of the

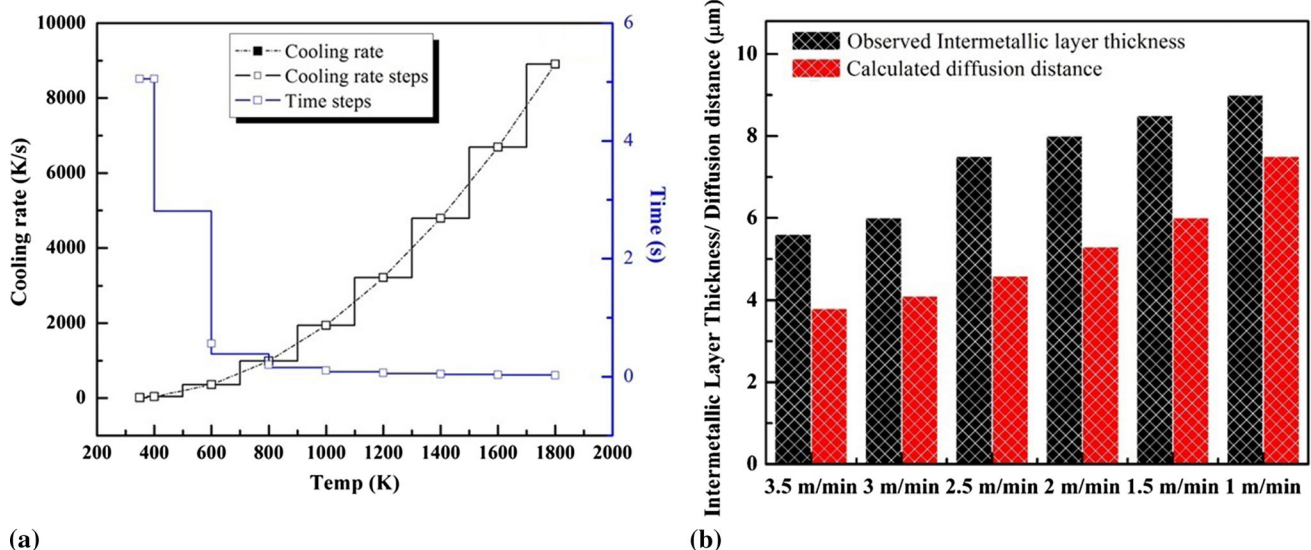


Fig. 8 (a) Cooling rates vs. Temperature at laser speed of 3.5 m/min (b) observed intermetallic layer thickness and calculated diffusion distance at different brazing scan speed

failure at steel interface confirms the detrimental effect of presence of intermetallic layer, as evident from Fig. 6(b). Though macrostructures (Fig. 1) of the joints revealed poor root filling with faster scan speed, favorable microstructure in terms of fineness and intermetallic layer thickness results in better mechanical properties of joints prepared with faster scan speed.

Figure 8(b) also shows that trends of calculated diffusion distance and observed intermetallic layer thickness with scan speed are same but deviation in magnitude is prominent. This variation may be attributed to the fact that intermetallic layer formation was not only restricted to diffusion controlled mechanism. Convective mass transfer in the molten filler pool was also a contributing factor for intermetallic layer formation. Therefore, the observed intermetallic layer thickness magnitude was more compared to calculated diffusion distance. Thus, layer thickness calculated by diffusion distance in previous research (Ref 15) may not be the sole mechanism for the same.

Wettability of the steel interface by the molten filler may also play crucial role in the joint strength as poor wettability leads to lower bonding capability. Zinc vaporization from the galvanized steel surface is important for understanding of this wetting behavior. Zn vaporization phenomenon can be described by Langmuir equation (Ref 25), where vaporization rate of a particular element at a specific temperature can be calculated using the following equation:

$$J = \frac{P^0}{\sqrt{2\pi MRT}} \quad (\text{Eq 4})$$

where  $J$  = vaporization flux in  $\text{mol/m}^2 \text{ s}$ ,  $P^0$  = vaporizing species' vapor pressure over the liquid ( $\text{Zn} = 23 \text{ Pa}$ ,  $\text{Al} = 1 \times 10^{-6} \text{ Pa}$ ) (Ref 23),  $M$  = molecular weight of the species ( $\text{Zn} = 65.38 \times 10^{-3} \text{ kg/mol}$ ,  $\text{Al} = 26.9815 \times 10^{-3} \text{ kg/mol}$ ) (Ref 18),  $R$  = universal gas constant ( $8.314 \text{ kJ/mol K}$ ) and  $T$  = temperature. The calculated vaporization rates at 1000 K of Zn and Al are  $4.099 \times 10^{-5}$  and  $2.8127 \times 10^{-12} \text{ mol/m s}$ , respectively. So, Zn vaporization rate is higher in multiple orders compared to aluminum and this leads to unfavorable surface tension value at steel interface. Evaporation of zinc results in increased surface energy, which makes galvanized steel thermodynamically unstable. Contact of molten metal with this unstable surface leads to limited wettability. Thus, higher evaporation rate may lead to poor joint strength. Lower welding speed leads to higher energy input, which may cause lower wettability (Ref 26) and accordingly, it can be a reason of decrease in joint strength. Thus, the joint strength trend presented in Fig. 6(a) can be accounted by this wettability decrease due to Zn evaporation along with the thickness variation of developed intermetallic layer.

## 4. Conclusions

In the present study, laser brazing experimentation and predictive model formulation for Laser brazing of aluminum alloy to steel was performed to correlate the welding parameters with the joint property through analyzing possible underlying mechanisms. The findings of the present investigation are summarized below:

1. Epitaxial growth at the aluminum side and intermetallic formation at steel interface were evident from microstructure of the brazed joint.
2. Better mechanical strength was observed in case of higher brazing speed.
3. Intermetallic layer thickness was found to be lower with increasing brazing speed as per experimental study; numerical results show similar trend in diffusion distance.
4. Along with intermetallic formation, zinc evaporation also affects joint strength. The tensile strength of brazed joint has reached a maximum value of 250 N/mm with a brazing speed of 3.5 m/min.

## Acknowledgments

Authors like to acknowledge Ms. Olga Simon of Fraunhofer-Institut für Werkstoff- und Strahltechnik IWS, Dresden, Germany, for her help to carry out some of the experimental work elaborated in the present study.

## References

1. L.H. Shah and M. Ishak, Review of Research Progress on Aluminum–Steel Dissimilar Welding, *Mater. Manuf. Process.*, 2014, **29**(8), p 928–933
2. G. Qin, Z. Lei, Y. Su, B. Fu, X. Meng, and S. Lin, Large Spot Laser Assisted GMA Brazing–Fusion Welding of Aluminum Alloy to Galvanized Steel, *J. Mater. Process. Technol.*, 2014, **214**(11), p 2684–2692
3. S. Katayama, Laser Welding of Aluminium Alloys and Dissimilar Metals, *Weld. Int.*, 2004, **18**(8), p 618–625
4. ASM Handbook Volume 3, *Alloy Phase Diagrams*. ISBN: 0-87170-381-5(v.3), p 77
5. L. Tricarico, R. Spina, D. Sorgente, and M. Brandizzi, Effects of Heat Treatments on Mechanical Properties of Fe/Al Explosion-Welded Structural Transition Joints, *Mater. Des.*, 2009, **30**(7), p 2693–2700
6. H. Oikawa, S. Ohmiya, T. Yoshimura, and T. Saitoh, Resistance Spot Welding of Steel and Aluminium Sheet Using Insert Metal Sheet, *Sci. Technol. Weld. Join.*, 1999, **4**(2), p 80–88
7. S. Wei, Y. Li, J. Wang, and K. Liu, Use of Welding–Brazing Technology on Microstructural Development of Titanium/Aluminium Dissimilar Joints, *Mater. Manuf. Process.*, 2014, **29**(8), p 961–968
8. W.B. Lee, M. Schmuecker, U.A. Mercardo, G. Biallas, and S.B. Jung, Interfacial Reaction in Steel–Aluminum Joints Made by Friction Stir Welding, *Scr. Mater.*, 2006, **55**(4), p 355–358
9. H.T. Zhang, J.C. Feng, P. He, and H. Hackl, Interfacial Microstructure and Mechanical Properties of Aluminium–Zinc-Coated Steel Joints Made by a Modified Metal Inert Gas Welding–Brazing Process, *Mater. Charact.*, 2007, **58**(7), p 588–592
10. R. Cao, Z. Feng, Q. Lin, and J.H. Chen, Study on Cold Metal Transfer Welding–Brazing of Titanium to Copper, *Mater. Des.*, 2014, **56**, p 165–173
11. M. Gatzten, T. Radel, C. Thomy, and F. Vollertsen, Wetting and Solidification Characteristic of Aluminium on Zinc Coated Steel in Laser Welding and Brazing, *J. Mater. Process. Technol.*, 2016, **238**, p 352–360
12. Y. Li, S. Hu, J. Shen, and B. Hu, Dissimilar Welding of H62 Brass-316L Stainless Steel Using Continuous-Wave Nd:YAG Laser, *Mater. Manuf. Process.*, 2014, **29**(8), p 916–921
13. A. Haboudou, P. Peyre, A.B. Vannes, and G. Peix, Reduction of Porosity Content Generated During Nd:YAG Laser Welding of A356 and AA5083 Aluminium Alloys, *Mater. Sci. Eng. A Struct.*, 2003, **363**(1), p 40–52



14. H. Laukant, C. Wallmann, M. Korte, and U. Glatzel, Flux-Less Joining Technique of Aluminium with Zinc-Coated Steel Sheets by a Dual-Spot-Laser Beam, *AMR*, 2005, **6**, p 163–170
15. V. Jindal, V.C. Srivastava, A. Das, and R.N. Ghosh, Reactive Diffusion in the Roll Bonded Iron–Aluminum System, *Mater. Lett.*, 2006, **60**(13), p 1758–1761
16. J. Liu, S. Jiang, Y. Shi, Y. Kuang, G. Huang, and H. Zhang, Laser Fusion–Brazing of Aluminum Alloy to Galvanized Steel with Pure Al Filler Powder, *Opt. Lasers Eng.*, 2015, **66**, p 1–8
17. R.W. Messler Jr., *Principles of Welding Processes, Physics, Chemistry and Metallurgy*, 2nd ed., Wiley-VCH Verlag GmbH and Co. KGaA, Weinheim, 2004, p 65, 163, 175
18. E.A. Brandes and G.B. Brook, *Smithells Metals Reference Book*, 7th ed., Reed Educational and Professional Publishing Limited, London, 1999, p 14–15
19. S. Patankar, *Numerical Heat Transfer and Fluid Flow*, CRC Press, Boca Raton, 1980, p 45
20. S. Kobayashi and T. Yakou, Control of Intermetallic Compound Layers at Interface Between Steel and Aluminum by Diffusion-Treatment, *Mater. Sci. Eng. A Struct.*, 2002, **338**(1), p 44–53
21. A. Kouadri-David and P.S.M. Team, Study of Metallurgic and Mechanical Properties of Laser Welded Heterogeneous Joints Between DP600 Galvanized Steel and Aluminium 6082, *Mater. Des.*, 2014, **54**, p 184–195
22. M. Windmann, A. Rottger, H. Kugler, W. Theisen, and F. Vollertsen, Laser Beam Welding of Aluminum to Al-Base Coated High-Strength Steel 22MnB5, *J. Mater. Process. Technol.*, 2015, **217**, p 88–95
23. S. Meco, G. Pardal, S. Ganguly, S. Williams, and N. McPherson, Application of Laser in Seam Welding of Dissimilar Steel to Aluminium Joints for Thick Structural Components, *Opt. Lasers Eng.*, 2015, **67**, p 22–30
24. J. Sun, Q. Yan, Z. Li, and J. Huang, Effect of Bevel Angle on Microstructure and Mechanical Property of Al/Steel Butt Joint Using Laser Welding–Brazing Method, *Mater. Des.*, 2016, **90**, p 468–477
25. T. DebRoy and S.A. David, Physical Processes in Fusion Welding, *Rev. Mod. Phys.*, 1995, **67**(1), p 85
26. C. Dharmendra, K.P. Rao, J. Wilden, and S. Reich, Study on Laser Welding–Brazing of Zinc Coated Steel to Aluminum Alloy with a Zinc Based Filler, *Mater. Sci. Eng. A Struct.*, 2011, **528**, p 1497–1503